# Disaggregation of Remotely Sensed Land Surface Temperature: A Generalized Paradigm

Yunhao Chen, Wenfeng Zhan, Jinling Quan, Ji Zhou, Xiaolin Zhu, and Hao Sun

***Abstract*—The environmental monitoring of earth surfaces requires land surface temperatures (LSTs) with high temporal and spatial resolutions. The disaggregation of LST (DLST) is an effective technique to obtain high-quality LSTs by incorporating two subbranches, including thermal sharpening (TSP) and temperature unmixing (TUM). Although great progress has been made on DLST, the further practice requires an in-depth theoretical paradigm designed to generalize DLST and then to guide future research before proceeding further. We thus proposed a generalized paradigm for DLST through a conceptual framework (*C-Frame*) and a theoretical framework (*T-Frame*). This was accomplished through a Euclidean paradigm starting from three basic laws summarized from previous DLST methods: the Bayesian theorem, Tobler's first law of geography, and surface energy balance. The *C-Frame* included a physical explanation of DLST, and the *T-Frame* was created by construing a series of assumptions from the three basic laws. Two concrete examples were provided to show the advantage of this generalization. We further derived the linear instance of this paradigm based on which two classical DLST methods were analyzed. This study finally discussed the implications of this paradigm to closely related topics in remote sensing. This paradigm develops processes to improve an understanding of DLST, and it could be used for guiding the design of future DLST methods.**

***Index Terms*—Disaggregation, generalized paradigm, land surface temperature (LST), temperature unmixing (TUM), thermal remote sensing, thermal sharpening (TSP).**

Manuscript received May 31, 2013; revised July 27, 2013; accepted November 23, 2013. Date of publication January 22, 2014; date of current version May 1, 2014. This work was supported in part by the National Natural Science Foundation of China under Grants 41071258 and 41301360, by the Natural Science Foundation of Jiangsu Province under Grant BK20130566, by the Open Fund of State Key Laboratory of Earth Surface Processes and Resource Ecology under Grant 2013-KF-01, by the Open Fund of State Key Laboratory of Remote Sensing Science under Grant OFSLRSS201214, by the Program for New Century Excellent Talents in University under Grant NCET-12-0057, by the Project of Science and Technology for Beijing Excellent Doctoral Dissertation Instructor under Grant 20131002702, and by the National 863 plan under Grant 2013AA122801.

Y. Chen, J. Quan, and H. Sun are with the State Key Laboratory of Earth Surface Processes and Resource Ecology, College of Resources Science and Technology, Beijing Normal University, Beijing 100875, China.

W. Zhan is with the Jiangsu Provincial Key Laboratory of Geographic Information Science and Technology, International Institute for Earth System Science, Nanjing University, Nanjing 210093, China, and also with the State Key Laboratory for Remote Sensing Science, Institute of Remote Sensing and Digital Earth, Chinese Academy of Sciences and Beijing Normal University, Beijing 100101, China (e-mail: zhanwenfeng1986@gmail.com).

J. Zhou is with the School of Resources and Environment, University of Electronic Science and Technology of China, Chengdu 610054, China.

X. Zhu is with the Department of Geography, The Ohio State University, Columbus, OH 43210-1361 USA.

Color versions of one or more of the figures in this paper are available online at http://ieeexplore.ieee.org.

Digital Object Identifier 10.1109/TGRS.2013.2294031

## I. Introduction

SATELLITE remote sensing provides a cost-effective way to monitor vast earth surfaces by mounting sensors on board satellites that are distant from surfaces. Due to the tradeoff among different sorts of resolution, no satellite sensor can provide data with high spatial resolution and, meanwhile, with high temporal and spectral resolutions, which leads to a mixture phenomenon in the temporal, spatial, and spectral domains. Because of the resolution tradeoff, efforts have been given over the past several decades to developing algorithms that could make satellite images more quantitatively accurate and easier for interpreters to decipher. Strahler *et al.* [1] predicted that, due to the relatively low spatial resolution of remotely sensed images, various methods would be proposed to infer the status of scenes using the available data at a larger scale of cell resolution (i.e., pixel level). These methods include the data fusion that began in the 1980s [2], was improved upon throughout the 1990s [3], and has been widely used since the 2000s, as reflected in the special issue on data fusion (see [4] and other papers in the same issue) these methods also include the spectral mixture analysis (SMA) that has experienced a similar development process (see [5] and other papers in the same issue).

As a crucial parameter for understanding the process of surface energy interactions, remotely sensed land surface temperature (LST) also experiences a similar paradoxical tradeoff of resolutions. Corresponding to image fusion and SMA, the disaggregation of LST (DLST) is of equal significance. In the past few decades, numerous investigations have been implemented, and great progress has been made for achieving DLST. In general, these studies can be divided into two broad categories: thermal sharpening (TSP) and temperature unmixing (TUM). These two categories have been shown to share similar predetermined assumptions, issues, and caveats, and they both inherit features from the subpixel analysis of optical images [6].

However, problems remain as DLST is evolving as one of the relatively independent research themes in the thermal remote sensing community: 1) DLST is still suffering a disorganized development because previous DLST methods have been evolving in different disciplines and because a thorough theoretical paradigm for DLST is in absence; 2) the empirical generalization of DLST is limited for understanding TSP and TUM as two subbranches of DLST; 3) most previous TSP methods sharpened the LSTs using the visible and near infrared (VNIR) images, which ignores that LST is responsive to the climatic and meteorological background associated with the land surface status, and LST fluctuates rapidly even in a diurnal temperature cycle (DTC), during which VNIR reflectance only changes slightly; in previous TUM, component temperatures

were mainly retrieved using the multiangle and multispectral thermal data, and the useful information provided by the multipixel and multitemporal thermal observations was usually disregarded; and 4) four predetermined principles, including the *additivity*, *separability*, *connectivity*, and *convertibility*, were raised by Zhan *et al.* [6]. These principles are necessary in most current DLST methods but were regularly unstated. How these principles may interact and how they may affect the design of better DLST methods remain vague. An in-depth theoretical exploration of these predetermined assumptions is thus in urgency.

Regarding these challenges and as DLST continues to progress and becomes more prevalent as one of the attractive topics [7], of great necessity is a theoretical and a generalized paradigm developed to fundamentally compact the roadbed of DLST before proceeding further. The design of DLST methods may be easier using a generalized paradigm rather than individuals' inspirations. This study is a continuation of that by Zhan *et al.* [6], and its intentions include the following: 1) to combine TSP and TUM theoretically; 2) to provide a generalized paradigm of DLST for guiding future research; and 3) to solidify DLST as a relatively independent research theme. This paper is not intended to either be a summary of the current DLST literature or demonstrate how a particular DLST method can be improved or how DLST is utilized in related applications. It is an attempt to identify the basic theory underlying all of the existing DLST methods that evolve from different disciplines, likening the identification of Newton's three laws of motion for classical mechanics.

Following this introduction, Section II provides the necessary definitions and three basic laws underlying DLST. A paradigmatic generalization for TSP and TUM is proposed in Section III, wherein two case studies are exemplified for deriving TSP and TUM and for illustrating the advantage of this generalized paradigm. Section IV further elucidates the ability of this paradigm based on which two classical DLST methods are derived. Discussions and conclusion are given in Sections V and VI, respectively.

## II. Background

### A. Definitions

*1) DLST, TSP, and TUM:* TSP and TUM are defined as two processes for estimating subpixel temperatures, wherein the former and the latter aim at the temperatures within regular subgrids or within irregular subareas, respectively. DLST is regarded as a generic process combining TSP and TUM [6].

*2) Background Temperature:* We term *background temperature* as the preliminary estimation of subpixel temperatures. In TSP, a background temperature represents the unsharpened temperature at low spatial resolutions; in TUM, it denotes the *a priori* component temperatures. Background temperature is a locally varying mean, and it is always inaccurate and thus becomes a basis for further estimation.

*1) Indirect Observation and Kernel: Indirect Observations* refer to measurements that are not directly related to LST but provide valuable information, and they can be used to infer the subpixel thermal status. In DLST, these indirect observations usually can be represented by VNIR images. A disaggregation *kernel* is defined as a derivative from indirect observations. For instance, the normalized difference vegetation index (NDVI) is a frequently used sharpening kernel due to its negative relationship with LST in most cases [8]; the angle-varying vegetation fraction observed from different directions is a prevalent unmixing kernel in the multiangle TUM [9], [10]. Note that the kernel herein inherits the concept of the kernel-driven model in the inversion of Moderate Resolution Imaging Spectroradiometer (MODIS)/albedo [11], which indicates the most important surface structure parameter that drives physical modeling. This definition is different from the kernel concept defined in image processing and machine learning. The kernel (i.e., moving window) in image processing is regularly used as a function of adjacent pixels [12]; while the kernel in machine learning generally aims at mapping data into a higher dimension space to facilitate statistical learning, best known in the support vector machine [13]. Disaggregation kernels have limitations although physically relating to LST. The relationship between kernels and LSTs sometimes is weak, and in this case, biases are inevitable.

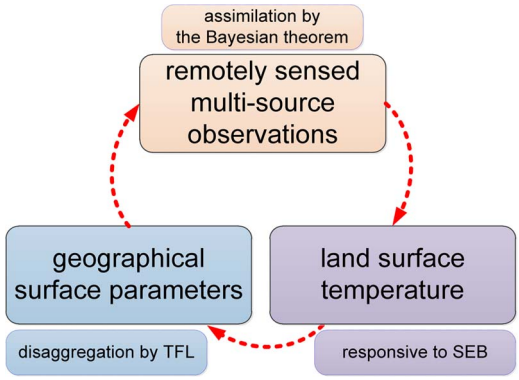


Fig. 1. Three laws involved in the DLST. TFL denotes Tobler's first law of geography, and SEB represents surface energy balance.

### B. Principal Laws

Three laws, including the Bayesian theorem, Tobler's first law of geography (TFL) [14], and the surface energy balance (SEB), are indispensable to DLST (see Fig. 1). The Bayesian theorem is a general framework for assimilating data of multiple sources; TFL describes the homogeneity and heterogeneity of the quantities of earth surfaces; and LST is the surface parameter that needs to be disaggregated, and it is a response to the SEB process.

*1) Law 1—Bayesian Theorem:* To obtain the optimal results of DLST, statistical inference is required for integrating multiple remotely sensed data; the Bayesian theorem is the key of statistical inference and links the *a priori* and *a posteriori* probability distribution functions (PDFs) of observations, expressed as

$$p(\mathbf{X}|\mathbf{Y}_{\text{obs}}) \propto p_{\text{B}}(\mathbf{X}) \cdot p(\mathbf{Y}_{\text{obs}}|\mathbf{X}) p^{-1}(\mathbf{Y}_{\text{obs}}) \qquad (1)$$

where $\mathbf{x}$ and $\mathbf{Y}_{\text{obs}}$ are the state variables and the new observations, respectively, $p_{\text{B}}(\mathbf{X})$ and $p(\mathbf{X}|\mathbf{Y}_{\text{obs}})$ are the *a priori* and *a posteriori* probabilities of state variables, and $p(\mathbf{Y}_{\text{obs}}|\mathbf{X})$ and $p(\mathbf{Y}_{\text{obs}})$ are the conditional and marginal probabilities of new observations. In DLST, $\mathbf{X}$ represents the temperature of subcomponents, and $\mathbf{Y}_{\text{obs}}$ denotes the observations relating to LST.

*2) Law 2—TFL:* The satellite observations that require a disaggregation are surface parameters. Generally, the geometry

and physical properties of the Earth's surfaces are diverse and distributed with a high degree of heterogeneity. Within a particular space, although specificity may exist, the distribution of surface parameters has a common spatial pattern. The understanding of this spatial pattern requires the knowledge of the TFL, which states that "*everything is related to everything else, but near things are more related than distant things*" [14]. Usually the observation model in DLST can be rewritten as

$$\mathbf{Y}_{\text{obs}} = \phi(\mathbf{T}_{\text{disag}}), \mathbf{T}_{\text{disag}} \in \Theta \tag{2}$$

where $\mathbf{T}_{\text{disag}}$ denotes the disaggregated subpixel temperatures, $\phi$ is the observation operator, and $\Theta$ represents the neighborhood area of any shape. From the perspective of DLST, the TFL has a twofold interpretation: 1) "*Near geographic entities are related*," which, for example, indicates that, in a relatively small area (i.e., $\Theta$ is local), the VNIR images that hold higher spatial resolutions are able to assist DLST, provided that LSTs are related to the VNIR-derived kernels statistically; and 2) "*near entities are more related than distance things*," which indicates that $\Phi$ is local and has a limited range. The TFL does not directly relate to $\phi$ but often plays a role confining $\Theta$ in which $\phi$ is statistically regressed. Within $\Theta$, the attributes of pixels such that LST has a solid statistical relationship with NDVI are regarded as invariant.

*3) Law 3—SEB:* The SEB model should be another basis for constructing the generalized paradigm of DLST. LST is responsive to the interactions of surface energy fluxes constrained by the SEB model; thus, it could be impacted by any factor that influences the surface energy budget, including the surface geometric structure and physical property and a variety of external factors such as weather and climate. The SEB equation is usually given as

$$Q_{\text{R}} = Q_{\text{H}} + Q_{\text{L}} + \text{Q}_{\text{G}} \tag{3}$$

where $Q_{\text{R}}$, $Q_{\text{H}}$, $Q_{\text{L}}$, and $Q_{\text{G}}$ are the net radiation, sensible, latent, and ground heat fluxes, respectively. Although energy balance is also related to the conservation of energy between the disaggregated coarse resolution radiance and the aggregated fine resolution radiance, this relation is not stressed because the conservation of energy has been satisfied automatically by the coupling of the Bayesian theorem and the TFL.

It is noteworthy that the Bayesian theorem, the TFL, and the SEB model have a progressively far-reaching relationship. The Bayesian theorem corresponds to the statistical inference based on multisource remote sensing data; the TFL corresponds to the spatial statistics inference over land surfaces; and the SEB model corresponds to the spatial statistics inference of LSTs, which are all contained in DLST (see Fig. 1). Therefore, it is understandable that these three laws match the three keywords in DLST, including "remotely sensed," "land surface," and "temperature," respectively.

## III. Generalized Paradigm

This section provides the generalized paradigm of DLST as two forms: *C-Frame* (conceptual framework) and *T-Frame* (theoretical framework). The *C-Frame* includes a physical explanation of DLST, and it conceptually generalizes features shared by TSP and TUM. Theoretical derivations are provided in their entirety as the *T-Frame*, which lists the generalized paradigm through deductions under a series of assumptions necessary for simplifying DLST.

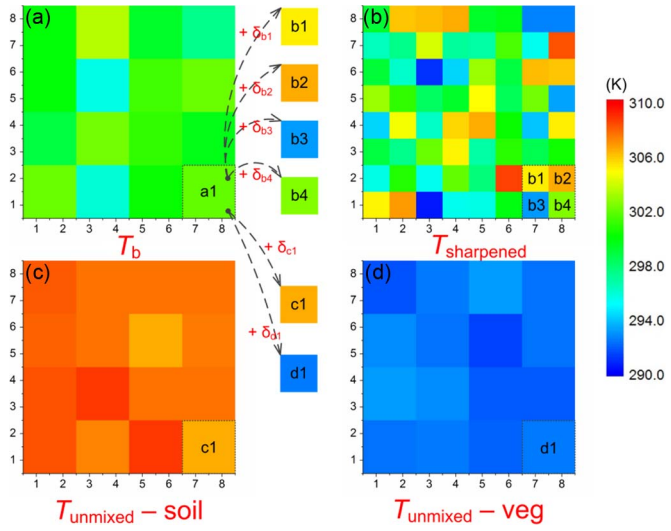


Fig. 2. Illustration of the conceptual framework of DLST. Assume that soil and vegetation are the only two land covers in this case study and the LST that needs disaggregation follows a uniform distribution between 290 K and 310 K. (a) is the simulated LST, (b) is the sharpened LST, (c) is the unmixed soil temperature, and (d) is the unmixed vegetation temperature. In TSP, Pixel a1 is sharpened into four subpixels, b1, b2, b3, and b4 through formulas, including $T_{\text{b1}} = T_{\text{a1}} + \delta_{\text{b1}}$, $T_{\text{b2}} = T_{\text{a1}} + \delta_{\text{b2}}$, $T_{\text{b3}} = T_{\text{a1}} + \delta_{\text{b3}}$, and $T_{\text{b4}} = T_{\text{a1}} + \delta_{\text{b4}}$. In TUM, Pixel a1 is unmixed into two component pixels, c1 and d1, using formulas, including $T_{\text{c1}} = T_{\text{a1}} + \delta_{\text{c1}}$ and $T_{\text{d1}} = T_{\text{a1}} + \delta_{\text{d1}}$.

### A. C-Frame

From a conceptual perspective, TSP and TUM share analogies in three aspects: 1) Intention—they both aim at disaggregating surface temperatures of a larger pixel into surface temperatures of several smaller components (e.g., disaggregating a1 into b1, b2, b3, and b4 in TSP or into c1 and d1 in TUM; see Fig. 2); 2) reasoning—they can both be perceived as a dynamic optimization problem that tries to estimate the disaggregated temperatures by assimilating the empirical estimates, multisource observations, and spatiotemporal models of surface temperatures; and 3) method—they both try to obtain the disaggregated temperatures by adding *background temperature* (or *a priori temperature*) and *thermal details* (e.g., adding $\delta_{\text{b1}}$, $\delta_{\text{b2}}$, $\delta_{\text{b3}}$, and $\delta_{\text{b4}}$ for TSP and adding $\delta_{\text{c1}}$ and $\delta_{\text{d1}}$ for TUM; see Fig. 2). TSP and TUM perform DLST with a similar intention, provide the theory of DLST through similar reasoning, and approach DLST using similar methods.

### B. T-Frame

The *T-Frame* consists of a list of formulas that generalizes TSP and TUM theoretically. These formulas are constructed from a number of increasingly stronger assumptions that are progressively increased by degree from $\text{A}_1$ to $\text{A}_3$ (see Fig. 3).

These assumptions include the Gaussian assumption $(\text{A}_1)$, which indicates that the errors of background temperature and indirect observations follow the normal distribution; the static assumption $(\text{A}_2)$, which indicates that all observations are synchronous; and the linear assumption $(\text{A}_3)$, which indicates an approximate linear relationship between temperatures and kernels.

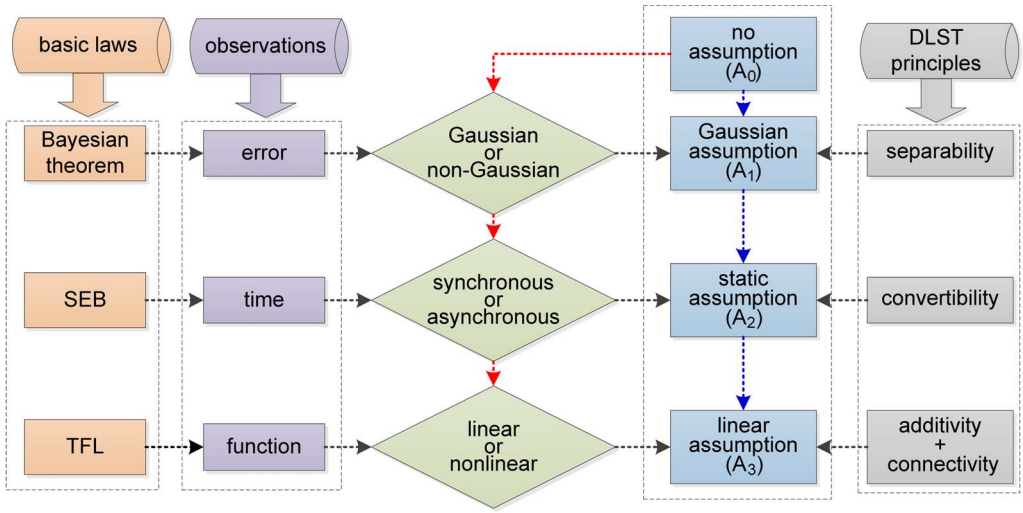


Fig. 3. Assumptions utilized in the theoretical framework of DLST. $A_0$ indicates that there is no assumption, $A_1$ is the Gaussian assumption, $A_2$ is the static assumption, and $A_3$ is the linear assumption.

Assumptions $A_1$, $A_2$, and $A_3$ correspond to the observation error, observation time, and observation function, respectively; and they further correspond to the Bayesian theorem, SEB, and TFL, respectively (see Fig. 3). Under the Bayesian theorem, the optimal disaggregated temperatures can be estimated by combining the background temperature and observations associated with their errors. With the SEB regulating the surface–atmosphere interactions, the temporal dynamics of LST can be derived. The observation function is describable through the TFL portraying the spatial patterns of both LSTs and disaggregation kernels. The TFL and the SEB fundamentally control the spatial and temporal behaviors of LSTs, respectively. This is different from the optical image fusion and SMA, in which optical reflectance changes more slowly in a DTC than the LSTs do, and thus, the temporal characteristics of optical reflectance in a DTC are less informative.

These three assumptions further relate to the principles of DLST given by Zhan *et al.* [6], including the *separability*, *convertibility*, *additivity*, and *connectivity* (see Fig. 3). The *separability* indicates whether the subcomponents are separable from a thermal perspective. This principle essentially challenges the homogeneous component assumption. This is because components would be inseparable if component temperatures are not single values but distribute in temperature intervals that overlap with each other. A Gaussian assumption (i.e., Assumption $A_1$) is usually used for differentiating the overlapped components and for determining the optimal disaggregated subpixel temperatures. The *convertibility* principle indicates that the temporal thermal observations (high temporal resolution) can be used to enhance the spatial resolution of LSTs if the temporal model of LST is established. Likewise, Assumption $A_2$ means that the LSTs are only disaggregated at an instantaneous moment, and the thermal observations that are temporally close to the current moment are disregarded. The *additivity* and *connectivity* principles suggest whether the disaggregation kernels are linearly or nonlinearly additive and that there are connections between kernels and LSTs. Assumption $A_3$ is a particular case of these two principles.

The *T-Frame* is represented in different forms under different assumptions (see Table I), and we provide this framework in the sequence of additional assumptions being satisfied.

TABLE I
THEORETICAL FRAMEWORK OF DLST UNDER DIFFERENT ASSUMPTIONS. "√" REPRESENTS THAT A CERTAIN ASSUMPTION IS SATISFIED, AND "×" REPRESENTS THE OPPOSITE

| Equations | Assumptions | | |
|---|---|---|---|
| | $A_1$ | $A_2$ | $A_3$ |
| Eq. (12) | √ | × | × |
| Eq. (13) | √ | √ | × |
| Eq. (15) | √ | √ | √ |

*1) Gaussian Assumption With Regard to the Bayesian Theorem:* Assumption $A_1$ is a predetermined assumption that is not openly stated but has been widely required in most DLST algorithms that employ the least square technique, although this assumption may induce slight biases, as evidenced by the geostationary satellite (GEOS) data [15], [16]. Using Advanced Spaceborne Thermal Emission and Reflection (ASTER)/LST as the ground truth at the spatial resolution of 90 m, we provide the error distributions of both background temperatures (i.e., MODIS/LST) and indirect estimations predicted using NDVI (see Fig. 4). The results confirm that the error distribution is approximately Gaussian, with the $R^2$ of 0.99, for both background temperatures and indirect observations. Moreover, the mean absolute error (MAE) between ASTER/LST and the unsharpened MODIS/LST alone is merely 1.52 K [see Fig. 4(a)]. An unexpected observation is that this error is already sufficiently low and comparable with the accuracy of most previous DLST methods [17]. This phenomenon commonly exists and indicates that simple criteria such as the MAE and root mean square deviation are insufficient for assessing disaggregation errors.

*a) Basic deductions:* Assume that the errors of background temperatures and indirect observations of LSTs are Gaussian distributed. The PDF of the background temperature can be described as follows:

$$\begin{cases} p_{\mathrm{B}}(\mathbf{T}_{\mathrm{disag}}) \propto (2\pi)^{-n/2}|\mathbf{\Sigma}_{\mathrm{d}}|^{-1/2}\exp\left[-\frac{1}{2}J_{\mathrm{b}}(\mathbf{T}_{\mathrm{disag}})\right] \\ J_{\mathrm{b}}(\mathbf{T}_{\mathrm{disag}}) = (\mathbf{T}_{\mathrm{disag}}-\mathbf{T}_{\mathrm{b}})^{\mathrm{T}}\mathbf{\Sigma}_{\mathrm{d}}^{-1}(\mathbf{T}_{\mathrm{disag}}-\mathbf{T}_{\mathrm{b}}) \end{cases} \quad (4)$$

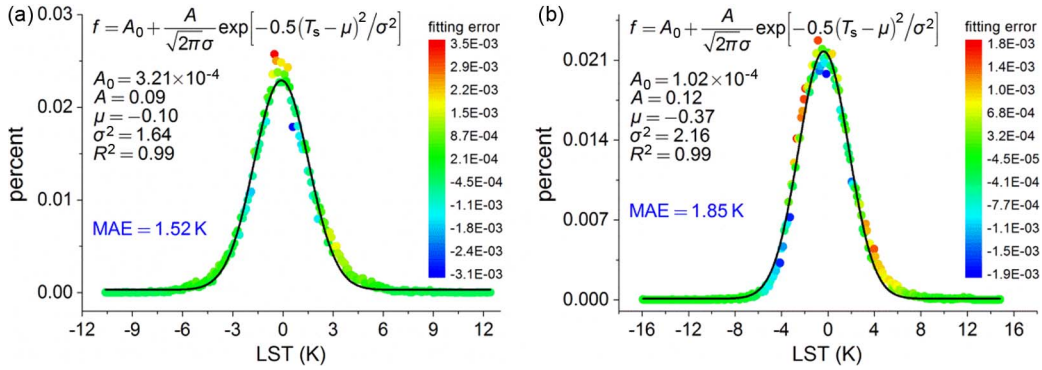


Fig. 4. (a) Error distributions of background temperature and (b) indirect observations predicted using NDVI. The errors were estimated using the comparisons between MODIS/LST and ASTER/LST at the spatial resolution of 90 m. The used data cover the urban areas of Beijing, acquired on August 31, 2004.

where $p_{\mathrm{B}}$ is the error PDF of the background temperature, $\mathbf{T}_{\mathrm{disag}}$ denotes the disaggregated temperatures, $\mathbf{T}_b$ is the background or the *a priori* temperature at low spatial resolution, $n$ is the number of subpixels or subcomponents, $\mathbf{\Sigma}_{\mathrm{d}}$ is the corresponding error covariance, and $J_{\mathrm{b}}$ is a predefined function. Similarly, the conditional PDF of indirect observations $\mathbf{Y}_{\mathrm{obs}}$ is expressed as

$$\begin{cases} p(\mathbf{Y}_{\mathrm{obs}}|\mathbf{T}_{\mathrm{disag}}) \\ \quad \propto (2\pi)^{-m/2}|\mathbf{\Omega}_{\mathrm{d}}|^{-1/2}\exp\left[-\frac{1}{2}J_{\mathrm{obs}}(\mathbf{T}_{\mathrm{disag}})\right] \\ J_{\mathrm{obs}}(\mathbf{T}_{\mathrm{disag}}) \\ \quad = \left[\mathbf{Y}_{\mathrm{obs}} - \phi_{\mathrm{d}}(\mathbf{T}_{\mathrm{diasg}})\right]^{\mathrm{T}}\mathbf{\Omega}_{\mathrm{d}}^{-1}\left[\mathbf{Y}_{\mathrm{obs}} - \phi_{\mathrm{d}}(\mathbf{T}_{\mathrm{disag}})\right] \end{cases} \tag{5}$$

where $p(\mathbf{Y}_{\mathrm{obs}}|\mathbf{T}_{\mathrm{disag}})$ is the conditional PDF of the observation error, $m$ is the number of observations, $\phi_{\mathrm{d}}$ and $\mathbf{\Omega}_{\mathrm{d}}$ are the observation operator and covariance, respectively, and $J_{\mathrm{obs}}$ is a predefined function. By incorporating a certain number of observations, the *a posteriori* PDF of the errors of disaggregated temperatures can be expressed as follows using the Bayesian theorem shown as (1):

$$\begin{cases} p(\mathbf{T}_{\mathrm{disag}}|\mathbf{Y}_{\mathrm{obs}}) \propto C(2\pi)^{-(m+n)/2}|\mathbf{\Sigma}|^{-1/2}|\mathbf{\Omega}|^{-1/2} \\ \quad \times \exp\left(-\frac{1}{2}\left[J_{\mathrm{b}}(\mathbf{T}_{\mathrm{disag}}) + J_{\mathrm{obs}}(\mathbf{T}_{\mathrm{disag}})\right]\right) \\ C = p^{-1}(\mathbf{Y}_{\mathrm{bos}}) \end{cases} \tag{6}$$

where $C$ is a constant. At this point, DLST is converted into a process of maximizing an *a posteriori* PDF, i.e., $\max P(\mathbf{T}_{\mathrm{disag}}|\mathbf{Y}_{\mathrm{obs}})$, which is equal to $\min J(\mathbf{T}_{\mathrm{disag}})$

$$\begin{aligned} \min J(\mathbf{T}_{\mathrm{disag}}) &= (\mathbf{T}_{\mathrm{disag}} - \mathbf{T}_{\mathrm{b}})^{\mathrm{T}}\mathbf{\Sigma}_{\mathrm{d}}^{-1}(\mathbf{T}_{\mathrm{disag}} - \mathbf{T}_{\mathrm{b}}) \\ &\quad + \left[\mathbf{Y}_{\mathrm{obs}} - \phi(\mathbf{T}_{\mathrm{disag}})\right]^{\mathrm{T}}\mathbf{\Omega}_{\mathrm{d}}^{-1}\left[\mathbf{Y}_{\mathrm{obs}} - \phi(\mathbf{T}_{\mathrm{disag}})\right] \end{aligned} \tag{7}$$

where $J(\mathbf{T}_{\mathrm{disag}})$ is the cost function. From the Bayesian perspective, we illustrate that the process of disaggregating temperatures is equivalent to minimizing $J(\mathbf{T}_{\mathrm{disag}})$. Therefore, DLST can be regarded as an optimization problem, and accordingly, numerous numerical tools developed by applied mathematicians can be employed to perform DLST.

*b) Generalization:* From a more generalized perspective, DLST is equivalent to "*determining a vector of disaggregated temperatures, which makes the distance between* $\mathbf{T}_{\mathrm{disag}}$ *and* $\mathbf{T}_{\mathrm{b}}$ *plus the distance between* $\phi_{\mathrm{d}}(\mathbf{T}_{\mathrm{disag}})$ *and* $\mathbf{Y}_{\mathrm{obs}}$ *the shortest*." The *distance* not only refers to the simple Euclidean distance but also indicates a more general concept such that the distance used in (7) is a form of Mahalanobis distance. This distance, in a broader sense, can be expressed in the norm form

$$\min J(\mathbf{T}_{\mathrm{disag}}) = \|\mathbf{T}_{\mathrm{disag}} - \mathbf{T}_{\mathrm{b}}\| + \|\mathbf{Y}_{\mathrm{obs}} - \phi_{\mathrm{d}}(\mathbf{T}_{\mathrm{disag}})\| \tag{8}$$

where $\|\cdot\|$ is the form of a norm.

*2) Static Assumption With Regard to the SEB:* LST is responsive to the net radiation $Q_{\mathrm{R}}$, soil heat flux $Q_{\mathrm{G}}$, and sensible and latent heat fluxes $Q_{\mathrm{H}}$ and $Q_{\mathrm{L}}$. By solving the heat conduction equation sandwiched by the SEB equation as the upper boundary and the constant thermal field as the lower boundary [18], a dynamic model that describes the temporal variation of LST can be derived. For the LST of a subpixel or a subcomponent, this dynamic model is written as

$$T = g(t) \tag{9}$$

where $g$ represents the dynamic model and $t$ is the time. In the dynamic model, LST is a function of the time, flux coefficients, and ground physical properties (e.g., thermal inertia). This model can be further converted into the following:

$$\begin{cases} T_{k+1} = g(t_{k+1}) \\ T_k = g(t_k) \end{cases} \Rightarrow T_{k+1} = \frac{g(t_{k+1})}{g(t_k)} \cdot T_k. \tag{10}$$

For a set of subcomponents, (10) can be further written as

$$\mathbf{T}_{k+1} = \mathbf{M}_k \cdot \mathbf{T}_k \tag{11}$$

where $\mathbf{T}_k$ and $\mathbf{T}_{k+1}$ are the subpixel LSTs at the $k$th and $(k+1)$th moments, respectively, and $\mathbf{M}$ is an operator that connects the thermal status of the previous and the following moments.

If the thermal observations are asynchronous (i.e., dynamic problem; see Fig. 5), (8) is then revised as [19]

$$\min J(\mathbf{T}_0) = \|\mathbf{T}_0 - \mathbf{T}_{\mathrm{b}}\| + \sum_{k=1}^{\mathrm{K}} \left\| \mathbf{Y}_{\mathrm{obs}}^k - \phi_{\mathrm{d}}^k \cdot \left( \prod_{i=0}^{k-1} \mathbf{M}_i \cdot \mathbf{T}_0 \right) \right\| \tag{12}$$

where $\mathbf{X}_0$ is the subcomponent temperature at the initial time, $\mathbf{K}$ is the number of time nodes, and $\mathbf{Y}_{\mathrm{obs}}^k$ and $\phi_{\mathrm{d}}^k$ are the observation value and observation operator at time $k$, respectively.

We provide an example of the dynamic DLST in Fig. 5, wherein the four MODIS/LSTs per daily cycle are combined and then disaggregated. Herein, the LST is considered dynamically changing with the SEB budget, and this dynamic model has been incorporated into the DLST process. Recent studies

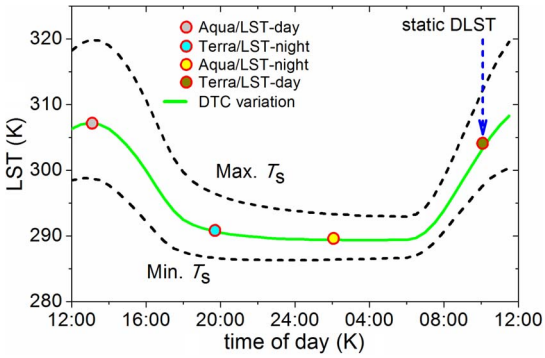


Fig. 5. Illustration of the dynamic and the static DLST in a DTC under clear sky. The static DLST suggests that the LSTs at a certain moment are disaggregated into higher spatial resolutions without the utilization of LSTs at other moments. The dynamic DLST means that the LSTs within an entire temperature cycle are disaggregated concurrently to obtain LSTs with both higher spatial and temporal resolutions. Max. $T_s$ and Min. $T_s$ are the maximum and minimum LSTs within a scene of LSTs, and $g(t)$ is the dynamic model of LST. The used data are acquired on August 31, 2004, and they cover the urban areas of Beijing.

have evidenced the importance of introducing the dynamic modeling into DLST by using multitemporal thermal data [20]. Note that the dynamic model can denote the LST variations not only in a DTC but also in an annual cycle [21].

Although the dynamic DLST is more useful and closer to reality than the static DLST, many classical DLST algorithms retrieved the subpixel or subcomponent temperatures at a single moment [10], [22]. The sharpening of Thematic Mapper/Enhanced Thematic Mapper Plus (TM/ETM+)LST is usually static because of its infrequent revisit; similarly, most previous studies sharpened the MODIS/LST and GEOS/LST statistically. A static assumption (Assumption $\mathrm{A}_2$) has been made implicitly in these algorithms, albeit multitemporal LSTs such as the daily Advanced Very High Resolution Radiometer (AVHRR)/LST and MODIS/LST have long been available.

For most previous DLST algorithms, the used observations are synchronous or quasi-synchronous (i.e., static problem), and (12) can then be simplified as follows:

$$\min J(\mathbf{T}_{\mathrm{disag}}) = \|\mathbf{T}_{\mathrm{disag}} - \mathbf{T}_{\mathrm{b}}\| + \|\mathbf{Y}_{\mathrm{obs}} - \phi_{\mathrm{d}}(\mathbf{T}_{\mathrm{disag}})\| \tag{13}$$

where $\mathbf{y}_{\mathrm{obs}}$ represents $\mathbf{Y}_{\mathrm{obs}}^{k}$. We term (12) and (13) as the generalized paradigm of DLST for the dynamic and static problems, respectively. Note that any form that satisfies the three conditions of designing a norm can be selected as specializations [23]. The simple Euclidean distance is not used as the only norm because other common norms, such as the spectral correlation measure, spectral angle mapping, and spectral information divergence, just to name a few, have also been frequently used and shown to be effective in related studies [24].

*3) Linear Assumption With Regard to the TFL:* Between disaggregation kernels and LSTs, there is usually a nonlinear relationship. This nonlinearity is so complex that an explicit expression may be difficult to provide. To date, there is still no strong evidence supporting whether the linearity or nonlinearity performs better [6]. This uncertainty is partly due to the kernel selection, which results in a reciprocity between the linear and nonlinear functions. For instance, a polynomial relationship between LSTs and kernels (i.e., NDVI and albedo) was provided to perform DLST, written as [25]

$$T_s = \sum_{n=0}^{4}\left(\sum_{j=0}^{n} a_{n,j}\cdot NDVI^{j}\cdot \alpha^{n-j}\right) \tag{14}$$

where $a$ and $\alpha$ represent the coefficient and albedo, respectively. Equation (14) is nonlinear when the NDVI and albedo are considered as two separate variables (i.e., kernels), but this relationship may be retransformed into a linear one when the disaggregation kernel is set as $NDVI^{j}\cdot\alpha^{n-j}$. The uncertainty between the linearity and nonlinearity is also partly due to the tradeoff of a function's abilities between regression and prediction. As a simple example, we provide a linear and a quadratic fitting between ASTER/LST and ASTER/NDVI over urban areas at the spatial resolution of 90 m (see Fig. 6). The statistics do show that the quadratic one is better than the linear one on regression, with a slightly higher $\mathrm{R}^2$. However, this slight improvement of accuracy is achieved at a price of the generalization ability, as the quadratic fitting is more oscillatory than the linear fitting as a result of the Runge phenomenon [26].

For simplicity, many previous studies assume that the disaggregation kernels are linearly related to LSTs, i.e., $\phi_{\mathrm{d}}$ is linear, which is not a true physical reality but practical in both TSP and TUM. Under this assumption, we then obtain the following solution of $\mathbf{T}_{\mathrm{disag}}$ [27]:

$$\mathbf{T}_{\mathrm{disag}} = \mathbf{T}_{\mathrm{b}} + \mathbf{\Sigma}_{\mathrm{d}}\phi_{\mathrm{d}}^{\mathrm{T}}\left(\mathbf{\Omega}_{\mathrm{d}} + \phi_{\mathrm{d}}\mathbf{\Sigma}_{\mathrm{d}}\phi_{\mathrm{d}}^{\mathrm{T}}\right)^{-1}\cdot\left(\mathbf{Y}_{\mathrm{obs}} - \phi_{\mathrm{d}}\mathbf{T}_{\mathrm{b}}\right) \tag{15}$$

where $\mathbf{T}_{\mathrm{disag}}$ is the disaggregated (i.e., sharpened or unmixed) temperatures. Equation (15) echoes the *C-Frame* of DLST: 1) TSP and TUM both utilize the background temperature at the spatial scale larger than the element; 2) they both estimate the thermal details using the weight factors multiplied by a kernel subtraction between the background pixel and subregions; and 3) subregions are either the subpixels in TSP or the subcomponents in TUM.

### C. Deductions of TSP and TUM

*1) TSP:* TSP is defined as a process through which LSTs are enhanced to higher spatial resolutions. In practice, LSTs are usually sharpened using two types of biased observations. The first concerns the rough observation at lower spatial resolutions; the other is the indirect observations used to deduce kernels at relatively higher spatial resolutions. We replace the DLST parameters in (15) with the TSP parameters, given as

$$\hat{\mathbf{T}}_{\mathrm{sharpened}} = \mathbf{T}_{\mathrm{b}} + \mathbf{\Sigma}_{\mathrm{s}}\phi_{\mathrm{s}}^{\mathrm{T}}\left(\mathbf{\Omega}_{\mathrm{s}} + \phi_{\mathrm{s}}\mathbf{\Sigma}_{\mathrm{s}}\phi_{\mathrm{s}}^{\mathrm{T}}\right)^{-1}\cdot\left(\rho_{\mathrm{high}} - \phi_{\mathrm{s}}\mathbf{T}_{\mathrm{b}}\right) \tag{16}$$

where $\hat{\mathbf{T}}_{\mathrm{sharpened}}$ denotes the estimated subpixel temperatures; $\mathbf{\Sigma}_{\mathrm{s}}$ and $\mathbf{\Omega}_{\mathrm{s}}$ are the covariance matrices of the background temperature and indirect observation; $\phi_{\mathrm{s}}$ is the observation operator, regularly inferred using the chosen VNIR kernels; and $\rho_{\mathrm{high}}$ is the sharpening kernel vector at high spatial resolutions. The key to sharpening LSTs is to determine the kernels and the corresponding covariance matrices.

In TSP, Zhan *et al.* [28] have demonstrated that the regression methods such as DisTrad [8] and TsHARP [22], the modulation methods such as PBIM [29] and S&C [30], and the hybrid

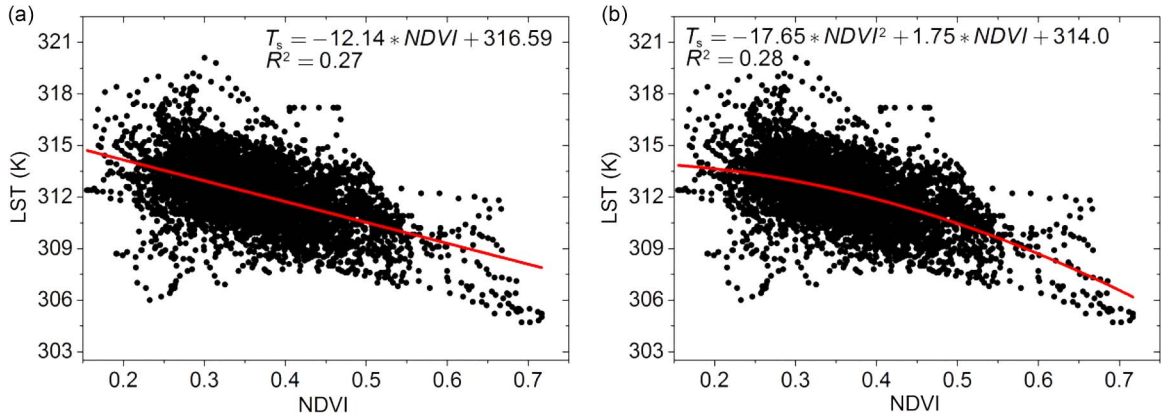


Fig. 6. Relationship between NDVI and LST. (a) represents a linear fitting, and (b) denotes a quadratic fitting. Sensor: ASTER. Location: Urban areas of Beijing. Spatial resolution: 90 m. Acquisition time: August 31, 2004.

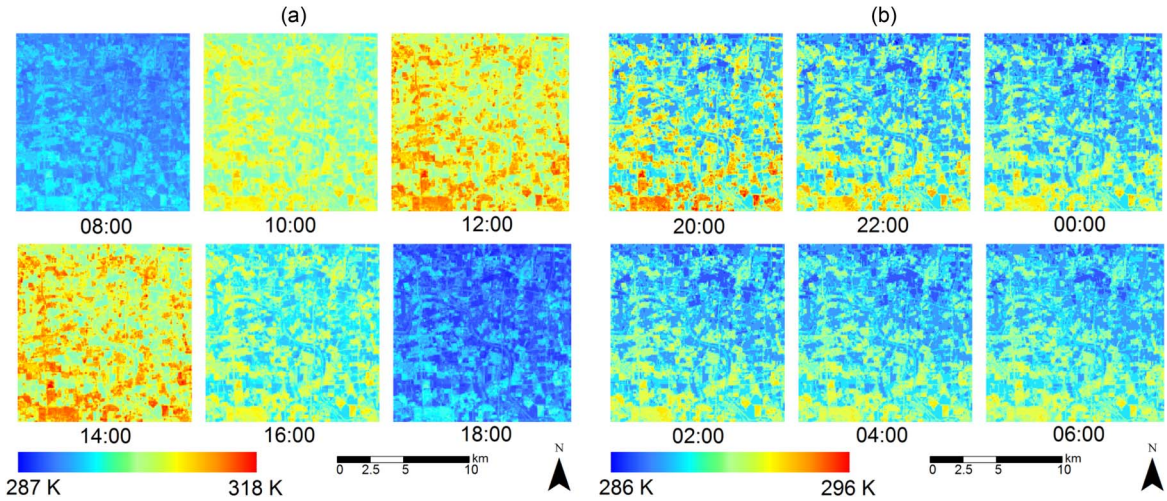


Fig. 7. Sharpening LSTs using the four daily MODIS/LSTs and ASTER/VNIR bands by coupling with the TFL and the SEB model. Spatial resolution: 90 m. Location: North of Beijing. (a) and (b) denote the daytime and nighttime sharpened LSTs, respectively. High-resolution LSTs were obtained at any time during a DTC, but only the LSTs are provided every 2 h for simplicity.

methods such as L&P [31] are all special cases of (16). The deduction of these methods starting from (16) indicates that Assumptions $A_1$ to $A_3$ have been made by default. The deduction of TSP shall resort to (13) when the $A_1$ and $A_2$ are satisfied but $A_3$ is unsatisfied, e.g., the utilization of piecewise functions [32] or intelligent statistical techniques to represent the relationship between kernels and LSTs. Equation (12) becomes the starting point for further deductions when both $A_2$ and $A_3$ are unsatisfied, e.g., the utilization of multitemporal thermal data [15], [33]. The recently developed methods that inherit from the DisTrad and TsHARP [34]–[36] have been succeeding under Assumptions $A_1$ and $A_2$.

Despite the fact that recent studies have incorporated the multitemporal data such as the GEOS/LST [15], strictly speaking, these methods are quasi-static because LSTs can only be sharpened at moments when low-resolution LSTs are available. Low-resolution LSTs derived from the SEB-based land surface model have also been integrated lately in TSP [37], but the SEB in these studies aims at producing background LSTs rather than coupling with TSP seamlessly.

Inspired by this paradigm, we provide a case study of sharpening the four MODIS/LSTs by coupling with the TFL and the SEB model (see Fig. 7). The corresponding histograms of the sharpened temperatures are given in Fig. 8. Relatively high-resolution LSTs (i.e., 90 m) are obtained at any time during a DTC. This case study shows that the incorporation of the SEB is important to TSP because LST is responsive to the surface energy budget. Moreover, the results confirm the following: 1) LST at a single pixel has a high variation in a DTC, and 2) daytime LSTs among pixels have a higher variance and

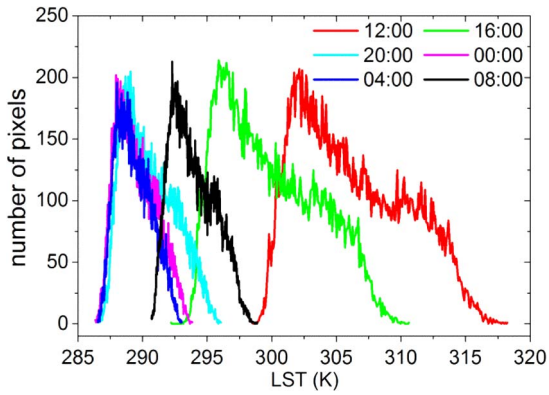


Fig. 8. Histograms of the sharpened LSTs at the resolution of 90 m at 00:00, 04:00, 08:00, 12:00, 16:00, and 20:00.

TABLE II
KEY OBSERVATION OPERATORS IN DIFFERENT TYPES OF TUM. "√" REPRESENTS A PARAMETER THAT VARIES WITH THE OBSERVATION CONDITION, AND "–" REPRESENTS A PARAMETER THAT IS A CONSTANT IN DIFFERENT OBSERVATION CONDITIONS

| Types | Component attributes | | |
|---|---|---|---|
| | fraction | emissivity | temperature |
| multiangle | √ | – | – |
| multispectral | – | √ | – |
| multitemporal | – | – | √ |
| multipixel | √ | – | √ |

distribute in a broader interval than nighttime LSTs (see Fig. 8), largely due to the thermal inertia differences among vegetation, soil, and impervious urban surfaces.

*2) TUM:* TUM is more straightforward than TSP, denoting a process of retrieving component temperatures using multiangle, multispectral, multipixel, or multitemporal observations. *Component* is a predetermined term that implies that the scene elements of remotely sensed images are both additive and separable. We replace the DLST parameters in (15) with the TUM parameters, written as

$$\hat{\mathbf{T}}_{\text{unmixed}} = \mathbf{T}_{\text{priori}} + \boldsymbol{\Sigma}_{\text{u}}\phi_{\text{u}}^{\text{T}}\left(\boldsymbol{\Omega}_{\text{u}} + \phi_{\text{u}}\boldsymbol{\Sigma}_{\text{u}}\phi_{\text{u}}^{\text{T}}\right)^{-1} \cdot\left[\mathbf{Y}_{\text{obs}} - \phi_{\text{u}}\mathbf{T}_{\text{priori}}\right] \quad (17)$$

where $\hat{\mathbf{T}}_{\text{unmixed}}$ is the unmixed component temperatures; $\mathbf{T}_{\text{priori}}$ is the *a priori* estimates of $\mathbf{T}_{\text{unmixed}}$, commonly represented by the rough estimates from the first iteration [38], by empirical values estimated from historical data, or by background estimations provided by land surface models [37]; $\Sigma_{\text{u}}$ and $\boldsymbol{\Omega}_{\text{u}}$ are the covariance matrices of the *a priori* estimates and observations, respectively; $\mathbf{y}_{\text{obs}}$ is the observations relating to the component temperatures; and $\phi_{\text{u}}$ is the corresponding observation operator.

We regard $\phi_{\text{u}}$ as the unmixing kernel, which resembles $\phi_{\text{s}}$ given in (16). $\phi_{\text{u}}$ varies with the observation condition and is the key to unmixing temperatures. The multiangle, multispectral, and multitemporal TUM becomes possible because the component fraction, emissivity, and temperature are angle dependent, spectrum dependent, and time dependent, respectively (see Table II) [9], [39]; the multipixel TUM is performed based on the spatially varying component fraction and temperature [40]. Assumption $\text{A}_2$ is satisfied in the multiangle, multispectral, and multipixel TUM. However, this assumption is invalidated by the multitemporal unmixing, which estimates component temperatures by dynamic modeling.

This paradigm stresses the combination of the three basic laws. Most previous methods tend to unmix component temperatures using either the multiangle or the multispectral thermal data. The statistical analysis of the multipixel data, which forms the basis of most classical TSP studies such as that by Agam *et al.* [22], has been rare in previous TUM. To show the advantage of this generalization, this study provides a case study of unmixing temperatures based on the TFL (see Figs. 9 and 10). In this example, the component temperatures are assumed to have a quadric distribution in local pixels [40]. The

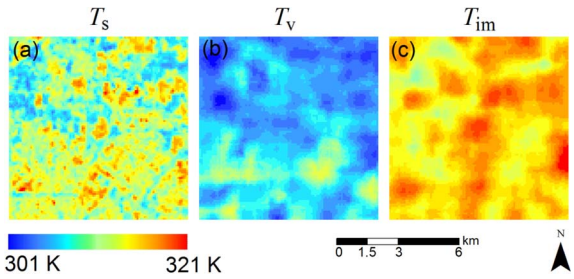


Fig. 9. Unmixing ASTER/LST by coupling with the TFL. (a) LST before TUM ($T_{\text{s}}$). (b) Unmixed vegetation temperature ($T_{\text{v}}$). (c) Unmixed temperature over impervious surface ($T_{\text{im}}$).

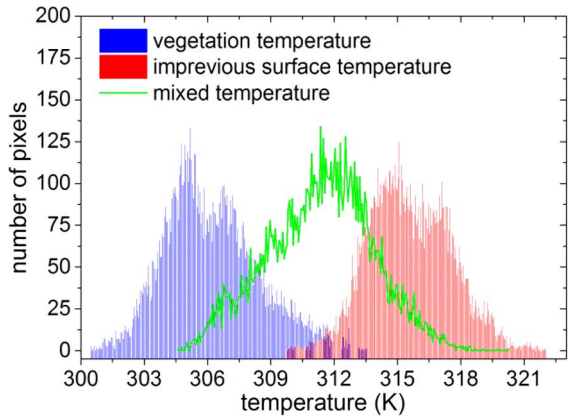


Fig. 10. Histograms of the mixed and the unmixed component LSTs.

ASTER/LSTs ($T_{\text{s}}$) are unmixed into only two components for simplicity, including vegetation ($T_{\text{v}}$) and impervious surface ($T_{\text{im}}$) because of the high temperature differences between these two components (see Fig. 10). These results confirm that the component temperatures can be unmixed by coupling with the TFL. Indeed, the SEB model has also been illustrated powerful to promote TUM [6]. As the satellite data from multiple sources continue to accumulate, the Bayesian theorem, together with the TFL and SEB, has further potential to enhance TUM.

### D. Precautions

First, with the global data involved in the derivation of the relationship between kernels and LSTs, both the prediction errors from the background temperatures and indirect observations have shown following the Gaussian distribution (see Fig. 4). However, recent studies found that, in particular cases, a local strategy that only includes the adjacent pixels within a small-size moving window for regression may be a better option for improving the DLST accuracy [35], [41]. In such cases, the locally small amount of data is likely to invalidate the Gaussian assumption (Assumption $\text{A}_1$) that is necessary for the deductions under the Bayesian theorem. This results in the recent incorporation of nonparametric methods that requires few samples, including the support vector machine, regression tree [35], and wavelet methods. Interestingly, these up-to-date algorithm developments on DSLT have been utilized in remote sensing image classification for long, which seemingly indicates a deep relation between DLST and image classification on both conceptualization and methodology (see Section V). Second, when applying the TFL, the static assumption (Assumption $\text{A}_2$) is also relevant. This is because the nearby geographical

entities are usually more related at a single moment, and land cover/land use dynamics may invalidate the close relations within nearby entities. Third, following the demonstration that most classical TSP algorithms, including, but not limited to, the regression method, the modulation method, and the hybrid method, are particular cases of a theoretical framework [28], this study further exemplifies that TSP and TUM share a common conceptual and theoretical basis. The successful generalization of TSP and TUM under a unified paradigm does not mean that the proposed paradigm is omnipotent but suggests that it is omnipresent. This paradigm has been demonstrated rooting in most DLST methods; it does not invalidate previous studies that the utilization of disaggregation kernels that are physically capable of relating LSTs to biophysical surface parameters is both practical and efficient for DLST.

### E. Deductions Under the Linear Assumption

This section continues to discuss the *T-Frame* of DLST when the linear assumption ($A_3$) is satisfied. The utilization of a single kernel for TSP (e.g., NDVI) is equivalent to the representation of two components in TUM (e.g., bare soil and crops involved over rural areas). Generally, $N$ kernels in TSP share equivalence with $N+1$ components in TUM. We divide the following deductions into two parts: 1) one kernel/two components and 2) two or more kernels/three or more components, because the case of two components in TUM is different from that of more than two components.

*1) Case 1—One Kernel/Two Components:*

*a) TSP:* If only one kernel is used, the process of TSP can be simplified from (16) as

$$\begin{aligned}\hat{T}_{\text{sharpened}} &= T_{\text{b}} + \sigma^2_{T_{\text{b}}}\left(\sigma^2_{T_{\text{b}}} + \sigma^2_{\phi_{\text{s}}(\rho_{\text{high}})}\right)^{-1} \cdot [\phi_{\text{s}}(\rho_{\text{high}}) - T_{\text{b}}] \\ &= T_{\text{b}} + \sigma^2_{T_{\text{b}}}\left(\sigma^2_{T_{\text{b}}} + \sigma^2_{\phi_{\text{s}}\rho_{\text{high}}}\right)^{-1} \cdot \phi_{\text{s}} \cdot (\rho_{\text{high}} - \rho_{\text{low}})\end{aligned} \tag{18}$$

where $\sigma^2_{T_{\text{b}}}$ and $\sigma^2_{\phi_{\text{s}}\rho_{\text{high}}}$ are the variances of background estimation and kernel prediction of sharpened temperatures, respectively, and $\rho_{\text{low}}$ is the kernel value at low spatial resolution.

*b) TUM:* One single thermal observation in TUM is expressed as follows when ignoring the internal reflections within a pixel:

$$f_1\varepsilon_1\phi_{\text{u}}(s,\lambda_1) + f_2\varepsilon_2\phi_{\text{u}}(s,\lambda_2) = T_{\text{b}} \tag{19}$$

where $f_1$, $f_2$, $\varepsilon_1$, $\varepsilon_2$, $\lambda_1$, and $\lambda_2$ are the component fraction, emissivity, and spatiotemporal parameters of the two components, respectively; and $s$ is the observational condition. In many occasions, $\phi_{\text{u}}(\cdot)$ is separable on the variables of $s$ and $\lambda$, indicating that $\phi_{\text{u}}(s,\lambda) = \phi'_{\text{u}}(s)\cdot\phi''_{\text{u}}(\lambda)$. One example of this kind of separation is the modeling of the spatial variation of component temperatures using polynomials in the multipixel TUM [40]. We thus obtain

$$f_1\varepsilon_1\phi'_{\text{u}}(s)\phi''_{\text{u}}(\lambda_1) + f_2\varepsilon_2\phi'_{\text{u}}(s)\phi''_{\text{u}}(\lambda_2) = T_{\text{b}} \tag{20}$$

where $\phi'_{\text{u}}(\cdot)$ and $\phi''_{\text{u}}(\cdot)$ are the two separated functions for $s$ and $\lambda$, respectively. Considering that $f_1 + f_2 = 100\%$, we then obtain

$$\begin{cases}\varepsilon_1\phi'_{\text{u}}(s)\phi''_{\text{u}}(\lambda_1) = T_{\text{b}} + \delta_1\cdot(f_1 - 100\%) \\ \varepsilon_2\phi'_{\text{u}}(s)\phi''_{\text{u}}(\lambda_2) = T_{\text{b}} + \delta_2\cdot(f_2 - 100\%)\end{cases} \tag{21}$$

where $f_1$ and $f_2$ are the kernel values at the level of the background pixel, 100% can be viewed as the kernel value at the subcomponent level because only one component exists in the corresponding subregion, and $\delta_1$ and $\delta_2$ are the weight factors of the first and second components, respectively, given by the following:

$$\begin{cases}\delta_1 = \phi'_{\text{u}}(s)\left[\varepsilon_2\phi''_{\text{u}}(\lambda_2) - \varepsilon_1\phi''_{\text{u}}(\lambda_1)\right] \\ \delta_2 = \phi'_{\text{u}}(s)\left[\varepsilon_1\phi''_{\text{u}}(\lambda_1) - \varepsilon_2\phi''_{\text{u}}(\lambda_2)\right].\end{cases} \tag{22}$$

Note that (18) and (21) have similar forms compared with (16) and (17), respectively. These equations share the same concept of DLST by adding background temperatures and thermal details.

*2) Case 2—Two or More Kernels/Three or More Components:*

*a) TSP:* The expression for TSP when two or more kernels are involved is derived as

$$\begin{aligned}T_{\text{sharpened}} = T_{\text{b}} + \sum_{k=1}^{N}\Bigg[&\sigma^2_{T_{\text{b}}}\left(\sigma^2_{T_{\text{b}}} + \sigma^2_{\phi^k_{\text{s}}\cdot\rho^k_{\text{high}}}\right)^{-1}\cdot\phi^k_{\text{s}} \\ &\cdot\left(\rho^k_{\text{high}} - \rho^k_{\text{low}}\right)\Bigg]\end{aligned} \tag{23}$$

where $\phi_k$ is the $k$th linear operator and $N$ is the kernel number.

*b) TUM:* The formula for TUM with $N+1$ components is provided as

$$\sum_{k=1}^{N+1} f_k\varepsilon_k\phi'_{\text{u}}(s)\phi''_{\text{u}}(\lambda_k) = T_{\text{b}}. \tag{24}$$

Given the condition that

$$f_i + \sum_{k=1,k\neq 1}^{N+1} f_k = 100\% \Rightarrow f_i = 100\% - \sum_{k=1,k\neq i}^{N+1} f_k \tag{25}$$

we then get

$$\begin{aligned}&\sum_{k=1,k\neq i}^{N+1} f_k\varepsilon_k\phi'_{\text{u}}(s)\phi''_{\text{u}}(\lambda_k) \\ &\quad + \left(100\% - \sum_{k=1,k\neq 1}^{N+1} f_k\right)[\varepsilon_i\phi'_{\text{u}}(s)\phi''_{\text{u}}(\lambda_i)] = T_{\text{b}} \\ &\Rightarrow \varepsilon_i\phi'_{\text{u}}(s)\phi''_{\text{u}}(\lambda_i) = T_{\text{b}} \\ &\quad + \sum_{k=1,k\neq 1}^{N+1} f_k\cdot[\varepsilon_i\phi'_{\text{u}}(s)\phi''_{\text{u}}(\lambda_i) - \varepsilon_k\phi'_{\text{u}}(s)\phi''_{\text{u}}(\lambda_k)].\end{aligned} \tag{26}$$

Equation (26) can be further simplified as

$$\begin{cases}\varepsilon_i\phi'_{\text{u}}(s)\phi''_{\text{u}}(\lambda_i) = T_{\text{b}} + \sum\limits_{k=1,k\neq i}^{N+1}\delta_k\cdot(f_k - 0\%) \\ \delta_k = \varepsilon_i\phi'_{\text{u}}(s)\phi''_{\text{u}}(\lambda_i) - \varepsilon_k\phi'_{\text{u}}(s)\phi''_{\text{u}}(\lambda_k)\end{cases} \tag{27}$$

where $\delta_k$ is the weight factor; 0% means the fraction of all the components within the $i$th subregion except the $i$th component itself.

Again, (23) (for TSP) and (27) (for TUM) correspond to (15) *C-Frame*, and they hold an analogous formula with the *T-Frame*.

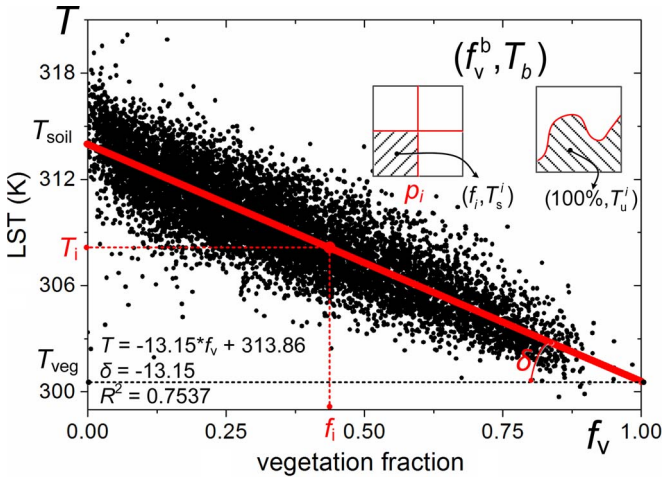


Fig. 11. Illustration of TSP and TUM through the approximate linear relationship between vegetation fraction and LST when assuming that there is no variation of soil moisture over surfaces. $f_{\rm v}^{\rm b}$ and $T_{\rm b}$ are the vegetation fraction and background temperature, respectively, $T_{\rm s}^i$ and $T_{\rm u}^i$ are the sharpened and unmixed temperatures of the $i$th subregion, respectively, and $T_{\rm soil}$ and $T_{\rm veg}$ are the unmixed soil and vegetation temperatures, respectively.

## IV. Derivation of Two Typical DLST Methods

This section demonstrates how two typical DLST methods are derived using the generalized paradigm. We selected several patches of rural areas southeast of Beijing as the study area, which is scattered with crops and bare soil. The remote sensing data are from Landsat-5/TM, acquired on July 6, 2004. The vegetation fraction was estimated using the NDVI method [42], and the LSTs were inverted using the monowindow method [43]. We chose one classical TSP method simplified from the study by Agam *et al.* [22] and Kustas *et al.* [8], and we chose one TUM method given by Sun *et al.* [44].

### A. Homogeneous Soil Moisture

The assumption of diagnostic homogeneity of soil moisture over adjacent pixels is partly reasonable. Many previous TSP [45], [46] and TUM studies [47], [48] have used this assumption. When assuming that there is no variation of soil moisture over the surfaces, the basic formulas for these two DLST methods are written as [22], [44]

$$\begin{cases} T_{\rm s}^i = T_{\rm b} + \delta \cdot \left(f_{\rm v}^{\rm b} - f_{\rm v}^i\right) \\ T_{\rm u}^i = T_{\rm b} + \delta \cdot \left(f_{\rm v}^{\rm b} - 100\%\right) \end{cases} \tag{28}$$

where $T_{\rm s}^i$ and $T_{\rm u}^i$ are the sharpened and unmixed temperatures of the $i$th subregion, respectively, $T_{\rm b}$ and $\delta$ are the background temperature and weight factor, respectively, $f_{\rm v}^{\rm b}$ and $f_{\rm v}^i$ are the vegetation fractions of the background pixel and the $i$th subregion, respectively, and 100% can be viewed as the vegetation fraction of the vegetation component.

An illustration in the case of no variation of soil moisture is provided in Fig. 11 through the approximate linear relationship between $f_{\rm v}$ and $T_{\rm s}$. Equation (28), associated with Fig. 11, demonstrates that these two DLST methods share a similar paradigm.

The first key step of Agam *et al.* [22] lies in the regression of a linear relationship between $f_{\rm v}$ and $T_{\rm s}$ using a group of pixels surrounding the object pixel. Although not noticeably stated, this step indicates that the surrounding pixels are homogeneous, which, however, does not mean that all the surrounding pixels are entirely consistent but represents that these pixels are just a composition of soil and vegetation with different proportions. The second key step is the modulation using background temperature (i.e., $T_{\rm b}$). These two steps allow for sharpening LSTs using a single formula of (28), which suggests an addition of the background temperature and the subtraction of kernel values weighted by the fitting slope (i.e., $\delta$).

From an intuitive perspective, TUM is just a separation of component temperatures unrelated to this paradigm. However, we demonstrate that the typical unmixing method developed by Sun *et al.* [44] connects the $T_{\rm s} - f_{\rm v}$ feature space. Using a transformed formula such as (28), TUM can be perceived as a process of adding the background temperature and thermal details that are determined by the subtraction of kernels multiplied again by the fitting slope (i.e., $\delta$).

### B. Heterogeneous Soil Moisture

In practice, the pixels that surround the object pixel may be diagnostically heterogeneous, e.g., the soil moisture varies with locations. This invalidates the linear relationship between $f_{\rm v}$ and $T_{\rm s}$, and it results in a triangle or trapezoid scatterplot in the $T{\rm s} - f_{\rm v}$ feature space (see Fig. 12).

Under this case, the formula for TSP [28] and the formula for TUM [44] can be rewritten as follows:

$$\begin{cases} T_{\rm s}^i = T_{\rm b} + \delta_{\rm dry} \cdot \tau_{\rm TVDI} \cdot \left(f_{\rm v}^{\rm b} - f_{\rm v}^i\right) \\ T_{\rm u}^i = T_{\rm b} + \delta_{\rm dry} \cdot \tau_{\rm TVDI} \cdot \left(f_{\rm v}^{\rm b} - 100\%\right) \end{cases} \tag{29}$$

where $\delta_{\rm dry}$ is the slope of the dry line and $\tau_{\rm TVDI}$ is the temperature vegetation dryness index (TVDI), an indicator that is based on the $T{\rm s} - f_{\rm v}$ relationship and represents the local soil moisture content, given by the following [49]:

$$\delta_{\rm dry} = \frac{T - T_{\min}}{T_{\max} - T_{\min}} \tag{30}$$

where $T_{\max}$ and $T_{\min}$ are the maximum and minimum temperatures at a certain NDVI, corresponding to the temperatures at the dry and wet lines in the feature space, respectively.

The key to DLST over areas with heterogeneous soil moisture is to extract the scatter shapes (e.g., borders and vertices) in the formulated $T_{\rm s} - f_{\rm v}$ space, a feature space construed by investigators to infer extra surface properties at least since the study by Goward *et al.* [50] and Carlson *et al.* [51]. This scatter shape, to some degree, represents the local physical properties of land surfaces (e.g., soil moisture), and it adds extra information for DLST other than what the kernel value at a single pixel could provide. No matter how the formulated shape may change, both TSP and TUM are a process of adding background temperatures and thermal details, although the multiplier of thermal details may change with the formulated shape. These results indicate that the process of DLST can be transformed into the determination of the multiplier of thermal details. The derivation of two seemingly different DLST methods, one from TSP and the other from TUM, under the unified paradigm, shows that this generalization has further potentials.

Component temperatures inverted from multiangle thermal observations have greatly advanced the estimation of

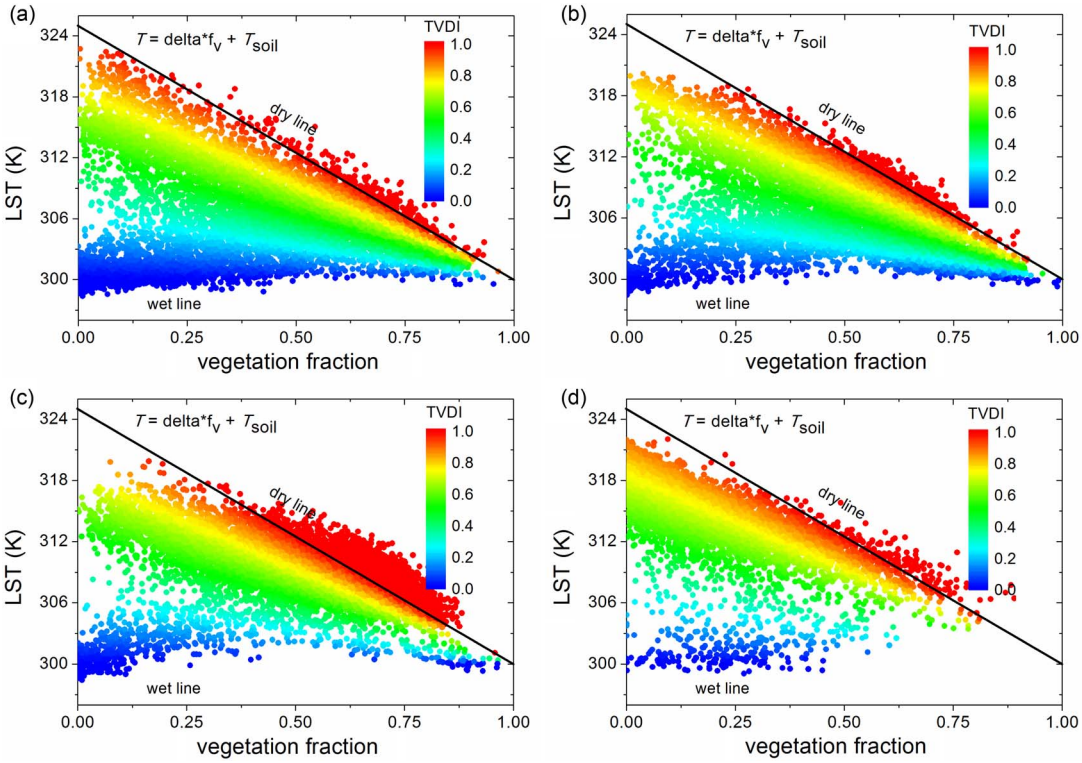


Fig. 12. Scatterplots in the $T_s - f_v$ space. The color represents the values of TVDI. The data of (a), (b), (c), and (d) are from different rural areas, scattering as approximate triangles in (a), (b), and (d) and as an approximate trapezoid in (c). The formulated shape is determined by the soil moisture and statistical range.

evapotranspiration by using the two-source model [52]. However, the design of a robust and practical method for inverting component temperatures from multiangle satellite thermal observations is not always easy because the vegetation structure and thermal anisotropy are difficult to parameterize at low spatial resolutions. A basic strategy for TSP is to exploit the information provided by adjacent pixels (i.e., TFL), based on which the relationship between kernels and LSTs is regressed statistically. The generalization of TSP and TUM under a unified paradigm indicates that the strategy of using TFL can be assimilated into TUM (also see Fig. 9). This strategy actually has been reflected in the multipixel TUM [40], [44]. This kind of TUM facilitates the inversion of component temperatures and thus can further assist the estimation of evapotranspiration. Interestingly, recent studies have resorted to apply the $T_s - f_v$ method directly to estimate surface energy fluxes [53], in which the TFL works and hides behind although not noticeably stated. Regarding the surface evapotranspiration estimation, the two-source model and the $T_s - f_v$ method are different in approach but are equally satisfactory in results. These analyses confirm the necessity of adopting the TFL and SEB as two basic laws supporting DLST, and they further illustrate the prospective of this paradigm on guiding future DLST.

## V. Discussion

### A. Indications Regarding DLST

This paradigm can be divided into three steps: 1) designing an optimization problem and the corresponding cost function equivalent to DLST; 2) seeking *a priori* knowledge about the disaggregated LSTs, whether from the background temperature, initial estimates, or other possible routines indicated in geophysical entities as an appearance of physical constraints and historical or empirical data that are linked to disaggregated temperatures; and 3) determining the elements within the covariance matrices of those formulas given in Table I, which directs to the optimal estimations of disaggregated LSTs. These three steps are *de facto* not new in the remote sensing community, where Verstraete *et al.* [54] once gave a general merit function to be minimized under an estimate of the least mean square. This was later echoed by Li *et al.* [11], stating the utilization of the Bayesian strategy for the accumulation of *a priori* knowledge, and then echoed by Wang [55], from which a regularization strategy was used. We further apply this strategy for structuring the theoretical basis of DLST and demonstrate that the kernel-driven concept is feasible in DLST at the scale of low spatial resolution.

### B. Indications Regarding Image Fusion and SMA

On the one hand, TSP and TUM are the two processes inheriting the attributes of image fusion and SMA, respectively [6]; therefore, this paradigm raises the possibility and lays foundations for the generalization of image fusion and SMA. This is because the subpixel analysis in thermal bands regarding temperature is more complex than that in optical bands regarding reflectance due to the highly dynamic nature of LST. Image fusion and SMA have been developed in parallel over the past four decades. Most image fusion (or image sharpening) methods, observed by Wang *et al.* [56] and the followers such as Dou *et al.* [57], can be assimilated. Recent work by Chen *et al.* [24] conveyed the possibility of assimilating the SMA methods using a more general distance (i.e., in the form of norm). There were also evidences implying the interoperability of

image fusion and SMA [58]–[60]. This interoperability, associated with the paradigm of DLST, predicts that a more extensive framework for generalizing image fusion and SMA is looming.

On the other hand, image fusion and SMA provide newly developed and advanced methods for TSP and TUM, respectively. For image fusion, the wavelet-based multiresolution method has been proved effective [61]. New disaggregation kernels that are based on the multiscale wavelet analysis of kernels rather than the simple band arithmetic (e.g., NDVI) can be designed, which may further enhance the current TSP. For SMA, spatial texture has been shown useful for improving the accuracy for long [62]; however, TUM does not attach importance to the spatial information among adjacent pixels until recently. The vertex component analysis (VCA) is powerful for unsupervised endmember extraction and for the determination of the simplex that encircles the scatters in the feature space [63]. In TUM, the VCA can be used to determine the dry and wet lines (see Fig. 8) that are crucial to DLST over areas with highly heterogeneous soil moisture.

### C. Indications Regarding Image Classification

The feature space technique involved in DLST is similar to that used in image processing such as the classification of multispectral remote sensing images. This similarity is not completely unexpected because there have been enough evidences supporting the resemblance between SMA and image classification [5]. Most approaches for image classification use the vertex of a scatterplot as the cluster center, and then, they classify those pixels near the cluster center to be in the same category as the cluster-center pixel. The comparability between DLST and image classification sheds light on the further extension of this paradigm.

Nevertheless, image classification is usually conducted at relatively high spatial resolutions, and it attempts to smooth the heterogeneity of pixels into homogeneous classes. By contrast, DLST is performed at relatively lower spatial resolutions, and it endows heterogeneity to those subcomponents within a larger background pixel. The bottom–up of image classification and the top–down of DLST meet, and these two processes are both depicted by the TFL, which incorporates the homogeneity as "*near things*" and incorporates the heterogeneity as "*distant things*" [14].

## VI. Conclusion

This study attempts to construct a Euclidean paradigm for DLST through a conceptual framework (*C-Frame*) and a theoretical framework (*T-Frame*). We try to be both theoretical and heuristic to illustrate the nature of DLST, although a lot of mathematics has been contained. We demonstrate that the two subbranches of DLST, i.e., TSP and TUM, can be generalized as two particular cases. The three laws, including the Bayesian theorem, TFL, and SEB, underlie DLST and fundamentally relate to most of the current DLST methods. Three assumptions that correspond to the three laws (e.g., the Gaussian assumption, static assumption, and linear assumption) are required to assist further deductions.

This study does not aim at designing a method that improves the DLST accuracy greatly or aim at replacing traditional DLST methods but aims at generalizing DLST and providing guidelines for further research through a broader perspective. From the Bayesian perspective, it is important to use and then integrate any potential observations under the Bayesian framework. In practice, however, this requires to design capable kernels that relate to LSTs through physical rendering. From the TFL's perspective, it is promising to incorporate the spatial statistical patterns of both kernels and LSTs to enhance DLST. From the SEB's perspective, incorporating the temporal dynamics of LSTs has further potentials because LST, by nature, is governed by the SEB process. As a driven and a responsive parameter of climatic factors, disaggregated LST would be meaningless until the instantaneous and average LSTs in a period are both captured.

This paradigm may also be illustrative for closely related fields in the remote sensing community. This study further indicates that the temporal, spatial, spectral, and angular resolutions of LST play their own individual parts as determinants of information sources in DLST. We suggest that the design strategy for thermal sensors on future satellites would be more powerful for monitoring environment if the sensors are designed to have multiple resolutions in different bands, by which great potential would then be yielded to fuse these types of images together to generate high-quality LSTs.

## References


[1] A. H. Strahler, C. E. Woodcock, and J. A. Smith, "On the nature of models in remote sensing," *Remote Sens. Environ.*, vol. 20, no. 2, pp. 121–139, Oct. 1986.

[2] J. C. Price, "Combining panchromatic and multispectral imagery from dual resolution satellite instruments," *Remote Sens. Environ.*, vol. 21, no. 2, pp. 119–128, Mar. 1987.

[3] C. Pohl and J. Van Genderen, "Multisensor image fusion in remote sensing: Concepts, methods and applications," *Int. J. Remote Sens.*, vol. 19, no. 5, pp. 823–854, Jan. 1998.

[4] P. Gamba and J. Chanussot, "Foreword to the special issue on data fusion," *IEEE Trans. Geosci. Remote Sens.*, vol. 46, no. 5, pp. 1283–1288, May 2008.

[5] A. Plaza, D. Du, J. Bioucas-Dias, X. Jia, and F. Kruse, "Foreword to the special issue on spectral unmixing of remotely sensed data," *IEEE Trans. Geosci. Remote Sens.*, vol. 49, no. 11, pp. 4103–4110, Nov. 2011.

[6] W. Zhan, Y. Chen, J. Zhou, J. Wang, W. Liu, J. Voogt, X. Zhu, J. Quan, and J. Li, "Disaggregation of remotely sensed land surface temperature: Literature survey, taxonomy, issues, caveats," *Remote Sens. Environ.*, vol. 131, pp. 119–139, Apr. 2013.

[7] M. C. Anderson, R. G. Allen, A. Morse, and W. P. Kustas, "Use of Landsat thermal imagery in monitoring evapotranspiration and managing water resources," *Remote Sens. Environ.*, vol. 122, pp. 50–65, Jul. 2012.

[8] W. P. Kustas, J. M. Norman, M. C. Anderson, and A. N. French, "Estimating subpixel surface temperatures and energy fluxes from the vegetation index-radiometric temperature relationship," *Remote Sens. Environ.*, vol. 85, no. 4, pp. 429–440, Jun. 2003.

[9] L. Jia, Z. L. Li, M. Menenti, Z. Su, W. Verhoef, and Z. Wan, "A practical algorithm to infer soil and foliage component temperatures from bi-angular ATSR-2 data," *Int. J. Remote Sens.*, vol. 24, no. 23, pp. 4739–4760, Jan. 2003.

[10] Z. L. Li, M. P. Stoll, R. H. Zhang, L. Jia, and Z. B. Su, "On the separate retrieval of soil and vegetation temperatures from ATSR data," *Sci. Chin. D, Earth Sci.*, vol. 44, no. 2, pp. 97–111, Feb. 2001.

[11] X. Li, J. Wang, F. Gao, and A. Strahler, "A priori knowledge accumulation and its application to linear BRDF model inversion," *J. Geophys. Res.*, vol. 106, no. D11, pp. 11 925–11 935, Jun. 2001.

[12] J. A. Richards, *Remote Sensing Digital Image Analysis*. New York, NY, USA: Springer-Verlag, 2012.

[13] V. Vapnik, *The Nature of Statistical Learning Theory*. Berlin, Germany: Springer-Verlag, 1999.

[14] W. R. Tobler, "A computer movie simulating urban growth in the Detroit region," *Econ. Geogr.*, vol. 46, pp. 234–240, Jun. 1970.

[15] B. Bechtel, K. Zakšek, and G. Hoshyaripour, "Downscaling land surface temperature in an urban area: A case study for Hamburg, Germany," *Remote Sens.*, vol. 4, no. 10, pp. 3184–3200, Oct. 2012.

[16] I. Keramitsoglou, C. T. Kiranoudis, and Q. Weng, "Downscaling geostationary land surface temperature imagery for urban analysis," *IEEE Geosci. Remote Sens. Lett.*, vol. 10, no. 5, pp. 1253–1257, Sep. 2013.

[17] W. Zhan, Y. Chen, J. Wang, J. Zhou, J. Quan, W. Liu, and J. Li, "Downscaling land surface temperatures with multi-spectral and multi-resolution images," *Int. J. Appl. Earth Observ. Geoinf.*, vol. 18, pp. 23–36, Aug. 2012.

[18] W. Zhan, Y. Chen, J. Voogt, J. Zhou, J. Wang, W. Liu, and W. Ma, "Interpolating diurnal surface temperatures of an urban facet using sporadic thermal observations," *Build. Environ.*, vol. 57, pp. 239–252, Nov. 2012.

[19] E. Kalnay, *Atmospheric Modeling, Data Assimilation and Predictability*. New York, NY, USA: Cambridge Univ. Press, 2002.

[20] J. Zhou, Y. H. Chen, X. Zhang, and W. F. Zhan, "Modeling the diurnal variations of urban heat island with multi-source satellite data," *Int. J. Remote Sens.*, vol. 34, no. 21, pp. 7568–7588, Nov. 2013.

[21] W. Zhan, J. Zhou, W. Ju, M. Li, I. Sandholt, J. Voogt, and C. Yu, "Remotely sensed soil temperatures beneath snow-free skin-surface using thermal observations from tandem polar-orbiting satellites: An analytical three-time-scale model," *Remote Sens. Environ.*, to be published.

[22] N. Agam, W. P. Kustas, M. C. Anderson, F. Li, and C. M. U. Neale, "A vegetation index based technique for spatial sharpening of thermal imagery," *Remote Sens. Environ.*, vol. 107, no. 4, pp. 545–558, Apr. 2007.

[23] E. Prugovecki, *Quantum Mechanics in Hilbert Space*. New York, NY, USA: Academic, 1981.

[24] J. Chen, X. Jia, W. Yang, and B. Matsushita, "Generalization of subpixel analysis for hyperspectral data with flexibility in spectral similarity measures," *IEEE Trans. Geosci. Remote Sens.*, vol. 47, no. 7, pp. 2165–2171, Jul. 2009.

[25] A. Dominguez, J. Kleissl, J. C. Luvall, and D. L. Rickman, "High-resolution Urban Thermal Sharpener (HUTS)," *Remote Sens. Environ.*, vol. 115, no. 7, pp. 1772–1780, Jul. 2011.

[26] J.-H. Jung and W. Stefan, "A simple regularization of the polynomial interpolation for the resolution of the Runge phenomenon," *J. Sci. Comput.*, vol. 46, no. 2, pp. 225–242, Feb. 2011.

[27] A. Tarantola, *Inverse Problem Theory and Methods for Model Parameter Estimation*. Philadelphia, PA, USA: SIAM, 2005.

[28] W. Zhan, Y. Chen, J. Zhou, J. Li, and W. Liu, "Sharpening thermal imageries: A generalized theoretical framework from an assimilation perspective," *IEEE Trans. Geosci. Remote Sens.*, vol. 49, no. 2, pp. 773–789, Feb. 2011.

[29] J. G. Liu and J. M. Moore, "Pixel block intensity modulation: Adding spatial detail to TM band 6 thermal imagery," *Int. J. Remote Sens.*, vol. 19, no. 13, pp. 2477–2491, Jan. 1998.

[30] M. Stathopoulou and C. Cartalis, "Downscaling AVHRR land surface temperatures for improved surface urban heat island intensity estimation," *Remote Sens. Environ.*, vol. 113, no. 12, pp. 2592–2605, Dec. 2009.

[31] D. Liu and R. Pu, "Downscaling thermal infrared radiance for subpixel land surface temperature retrieval," *Sensors*, vol. 8, no. 4, pp. 2695–2706, Apr. 2008.

[32] L. Jing and Q. Cheng, "A technique based on non-linear transform and multivariate analysis to merge thermal infrared data and higher-resolution multispectral data," *Int. J. Remote Sens.*, vol. 31, no. 24, pp. 6459–6471, Dec. 2010.

[33] K. Zakšek and K. Oštir, "Downscaling land surface temperature for urban heat island diurnal cycle analysis," *Remote Sens. Environ.*, vol. 117, pp. 114–124, Feb. 2011.

[34] W. Essa, J. van der Kwast, B. Verbeiren, and O. Batelaan, "Downscaling of thermal images over urban areas using the land surface temperature-impervious percentage relationship," *Int. J. Appl. Earth Observ. Geoinf.*, vol. 23, pp. 95–108, Aug. 2013.

[35] F. Gao, W. P. Kustas, and M. C. Anderson, "A data mining approach for sharpening thermal satellite imagery over land," *Remote Sens.*, vol. 4, no. 11, pp. 3287–3319, Oct. 2012.

[36] S. Zhu, H. Guan, A. C. Millington, and G. Zhang, "Disaggregation of land surface temperature over a heterogeneous urban and surrounding suburban area: A case study in Shanghai, China," *Int. J. Remote Sens.*, vol. 34, no. 5, pp. 1707–1723, Mar. 2013.

[37] A. Kallel, C. Ottle, S. Le Hegarat-Mascle, F. Maignan, and D. Courault, "Surface temperature downscaling from multiresolution instruments based on Markov models," *IEEE Trans. Geosci. Remote Sens.*, vol. 51, no. 3, pp. 1588–1612, Mar. 2013.

[38] Q. Liu, X. Z. Xin, R. R. Deng, Q. Xiao, Q. H. Liu, and G. L. Tian, "Retrieve component temperature for wheat field with ASTER image," in *Proc. IEEE IGARSS*, Jun. 2002, vol. 6, pp. 3680–3682.

[39] X. Song and Y. Zhao, "Study on component temperatures inversion using satellite remotely sensed data," *Int. J. Remote Sens.*, vol. 28, no. 11, pp. 2567–2579, May 2007.

[40] W. Zhan, Y. Chen, J. Zhou, and J. Li, "An algorithm for separating soil and vegetation temperatures with sensors featuring a single thermal channel," *IEEE Trans. Geosci. Remote Sens.*, vol. 49, no. 5, pp. 1796–1809, May 2011.

[41] C. Jeganathan, N. Hamm, S. Mukherjee, P. M. Atkinson, P. Raju, and V. Dadhwal, "Evaluating a thermal image sharpening model over a mixed agricultural landscape in India," *Int. J. Appl. Earth Observ. Geoinf.*, vol. 13, no. 2, pp. 178–191, Apr. 2011.

[42] J. A. Sobrino, J. C. Jiménez-Muñoz, and L. Paolini, "Land surface temperature retrieval from LANDSAT TM 5," *Remote Sens. Environ.*, vol. 90, no. 4, pp. 434–440, Apr. 2004.

[43] Z. Qin, A. Karnieli, and P. Berliner, "A mono-window algorithm for retrieving land surface temperature from Landsat TM data and its application to the Israel-Egypt border region," *Int. J. Remote Sens.*, vol. 22, no. 18, pp. 3719–3746, Jan. 2001.

[44] Z. Sun, Q. Wang, B. Matsushita, T. Fukushima, Z. Ouyang, and M. Watanabe, "A new method to define the VI-Ts diagram using subpixel vegetation and soil information: A case study over a semiarid agricultural region in the north China plain," *Sensors*, vol. 8, no. 10, pp. 6260–6279, Oct. 2008.

[45] T. Bellerby, M. Taberner, A. Wilmshurst, M. Beaumont, E. Barrett, J. Scott, and C. Durbin, "Retrieval of land and sea brightness temperatures from mixed coastal pixels in passive microwave data," *IEEE Trans. Geosci. Remote Sens.*, vol. 36, no. 6, pp. 1844–1851, Nov. 1998.

[46] G. I. Sentlinger, S. J. Hook, and B. Laval, "Sub-pixel water temperature estimation from thermal-infrared imagery using vectorized lake features," *Remote Sens. Environ.*, vol. 112, no. 4, pp. 1678–1688, Apr. 2008.

[47] J. Dozier, "A method for satellite identification of surface temperature fields of subpixel resolution," *Remote Sens. Environ.*, vol. 11, pp. 221–229, Jan. 1981.

[48] R. Zhang, J. Tian, H. Su, X. Sun, S. Chen, and J. Xia, "Two improvements of an operational two-layer model for terrestrial surface heat flux retrieval," *Sensors*, vol. 8, no. 10, pp. 6165–6187, Oct. 2008.

[49] I. Sandholt, K. Rasmussen, and J. Andersen, "A simple interpretation of the surface temperature/vegetation index space for assessment of surface moisture status," *Remote Sens. Environ.*, vol. 79, no. 2/3, pp. 213–224, Feb. 2002.

[50] S. N. Goward, G. D. Cruickshanks, and A. S. Hope, "Observed relation between thermal emission and reflected spectral radiance of a complex vegetated landscape," *Remote Sens. Environ.*, vol. 18, no. 2, pp. 137–146, Oct. 1985.

[51] T. N. Carlson, R. R. Gillies, and E. M. Perry, "A method to make use of thermal infrared temperature and NDVI measurements to infer surface soil water content and fractional vegetation cover," *Remote Sens. Rev.*, vol. 9, no. 1/2, pp. 161–173, Mar. 1994.

[52] J. M. Norman, W. P. Kustas, and K. S. Humes, "Source approach for estimating soil and vegetation energy fluxes in observations of directional radiometric surface temperature," *Agr. Forest Meteorol.*, vol. 77, no. 3/4, pp. 263–293, Dec. 1995.

[53] R. Tang, Z.-L. Li, and B. Tang, "An application of the Ts-VI triangle method with enhanced edges determination for evapotranspiration estimation from MODIS data in arid and semi-arid regions: Implementation and validation," *Remote Sens. Environ.*, vol. 114, no. 3, pp. 540–551, Mar. 2010.

[54] M. M. Verstraete, B. Pinty, and R. B. Myneni, "Potential and limitations of information extraction on the terrestrial biosphere from satellite remote sensing," *Remote Sens. Environ.*, vol. 58, no. 2, pp. 201–214, Nov. 1996.

[55] Y. F. Wang, "Quantitative remote sensing inversion in earth science: Theory and numerical treatment," in *Handbook of Geomathematics*, W. Freeden, Z. Nashed, and T. Sonar, Eds. Berlin, Germany: Springer-Verlag, 2010, pp. 785–812.

[56] Z. Wang, D. Ziou, C. Armenakis, D. Li, and Q. Li, "A comparative analysis of image fusion methods," *IEEE Trans. Geosci. Remote Sens.*, vol. 43, no. 6, pp. 1391–1402, Jun. 2005.

[57] W. Dou, Y. Chen, X. Li, and D. Z. Sui, "A general framework for component substitution image fusion: An implementation using the fast image fusion method," *Comput. Geosci.*, vol. 33, no. 2, pp. 219–228, Feb. 2007.

[58] H. N. Gross and J. R. Schott, "Application of spectral mixture analysis and image fusion techniques for image sharpening," *Remote Sens. Environ.*, vol. 63, no. 2, pp. 85–94, Feb. 1998.

[59] W. Yang, J. Chen, B. Matsushita, M. G. Shen, and X. H. Chen, "Practical image fusion method based on spectral mixture analysis," *Sci. Chin. Inf. Sci.*, vol. 53, no. 6, pp. 1277–1286, Jun. 2010.
[60] G. D. Robinson, H. N. Gross, and J. R. Schott, "Evaluation of two applications of spectral mixing models to image fusion," *Remote Sens. Environ.*, vol. 71, no. 3, pp. 272–281, Mar. 2000.
[61] J. Nunez, X. Otazu, O. Fors, A. Prades, V. Pala, and R. Arbiol, "Multiresolution-based image fusion with additive wavelet decomposition," *IEEE Trans. Geosci. Remote Sens.*, vol. 37, no. 3, pp. 1204–1211, May 1999.
[62] A. Plaza, P. Martinez, R. Pérez, and J. Plaza, "Spatial/spectral endmember extraction by multidimensional morphological operations," *IEEE Trans. Geosci. Remote Sens.*, vol. 40, no. 9, pp. 2025–2041, Sep. 2002.
[63] J. M. Nascimento and J. B. Dias, "Vertex component analysis: A fast algorithm to unmix hyperspectral data," *IEEE Trans. Geosci. Remote Sens.*, vol. 43, no. 4, pp. 898–910, Apr. 2005.

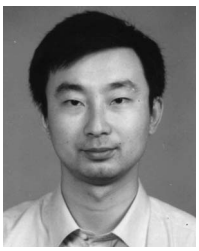

**Yunhao Chen** received the B.S. and M.S. degrees in resource management from the Anhui University of Science and Technology, Huainan, China, in 1994 and 1997, respectively, and the Ph.D. degree in geodesic engineering from the China University of Mining and Technology, Beijing, China, in 1999.

He is currently a Professor at Beijing Normal University, Beijing, China, and a Special Research Scholar of the National Disaster Reduction Committee, Ministry of Civil Affairs of China. From 2000 to 2001, he did postdoctoral research in Beijing Normal University. From 2001 up to the present, he has been with the College of Resource Science and Technology, Beijing Normal University. His research interests include thermal remote sensing applications in urban heat island phenomena, evapotranspiration, and natural disaster reduction.

**Wenfeng Zhan** received the B.S. degree in photogrammetry and remote sensing from Wuhan University, Wuhan, China, in 2007 and the Ph.D. degree from the College of Resources Science and Technology, Beijing Normal University, Beijing, China, in 2012.

He is currently an Associate Professor with the International Institute for Earth System Science, Nanjing University, Nanjing, China. His main research focuses on the urban heat island, thermal anisotropy, and disaggregation of land surface temperature.

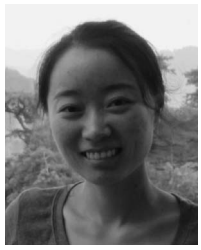

**Jinling Quan** received the B.E. degree in surveying engineering from the College of Civil Engineering, Tongji University, Shanghai, China, in 2010. She is currently working toward the Ph.D. degree in the College of Resources Science and Technology, Beijing Normal University, Beijing, China.

Her research focuses on the application of geographic information systems and remote sensing of urban environment.

**Ji Zhou** received the B.S. degree in geographic information system from Nanjing University, Nanjing, China, in 2005 and the Ph.D. degree in remote sensing from Beijing Normal University, Beijing, China, in 2010.

He was a Visiting Ph.D. Student in the Department of Geography, University of Western Ontario, London, ON, Canada, from October 2008 to April 2009 and was an Assistant Professor with the School of Resources and Environment (SRE), University of Electronic Science and Technology of China (UESTC), Chengdu, China, from July 2010 to July 2012. He is currently an Associate Professor with SRE, UESTC. His research focuses on the thermal remote sensing of land surfaces, including the estimation of land surface temperatures and component temperatures, spatial and temporal gap filling of thermal remote sensing data, and the analysis of urban heat islands.

**Xiaolin Zhu** received the B.S. degree in resource science and engineering and the M.E. degree in civil engineering from Beijing Normal University, Beijing, China, in 2007 and 2010, respectively. He is currently working toward the Ph.D. degree in geography at The Ohio State University, Columbus, OH, USA.

His research interests include remote sensing image processing and quantitative information retrieval. In particular, he has been doing research to enhance the remotely sensed data, such as filling gaps in Scan Line Corrector (SLC)-off Landsat-7 ETM+ images, blending images from multisources, and removing cloud contamination. He is also interested in land-surface parameter retrieval, such as estimating forest composition and structural parameters.

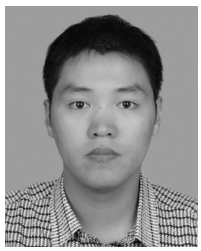

**Hao Sun** received the B.S. and M.S. degrees in geographical information system from the China University of Mining and Technology, Xuzhou, China, in 2008 and 2011, respectively. He is currently working toward the Ph.D. degree in the College of Resources Science and Technology, Beijing Normal University, Beijing, China.

His research focuses on the application of GIS and remote sensing.